Nano Energy 103 (2022) 107793

Contents lists available at ScienceDirect

Nano Energy

journal homepage: www.elsevier.com/locate/nanoen

Understanding morphology effects on fill factor losses in dilute-donor organic solar cells

Aaron Kramer [a], Waldemar Kaiser [b], Boya Zhang [c], Lakshmi N.S. Murthy [c], Alessio Gagliardi [d], Julia W.P. Hsu [c,*], William G. Vandenberghe [c,*]

[a] Department of Physics, University of Texas at Dallas, 800 West Campbell Road, Richardson, TX 75080, USA
[b] Computational Laboratory for Hybrid/Organic Photovoltaics (CLHYO), Istituto CNR di Scienze e Tecnologie Chimiche "Giulio Natta" (CNR-SCITEC), 06123 Perugia, Italy
[c] Department of Materials Science and Engineering, University of Texas at Dallas, 800 West Campbell Road, Richardson, TX 75080, USA
[d] Department of Electrical and Computer Engineering, Technical University of Munich, Arcisstrasse 21, 80333 Munich, Germany

ARTICLE INFO

Keywords:
Fill factor
Morphology
Organic Solar Cells
Dilute-Donor
Polymers
Small molecules

ABSTRACT

Experimental results of organic solar cells with low donor concentrations using small molecule donors have displayed significantly lower fill factors (FFs) compared to dilute-donor solar cells (DDSCs) with polymer donors. We perform experiments and kinetic Monte Carlo simulations, to understand the observed FF discrepancy and how FF can be improved. Our results reveal that small molecule DDSCs collect holes from the region of the active layer near the anode whereas polymer DDSCs collect holes from a deeper volume inside the active layer. This enlarged collection region is facilitated by the morphology of polymer chains extending from the anode into the active layer. The chains permit holes to hop along the donor sites to the anode with no barrier. Small molecule DDSCs, in contrast, require a large electric field to transfer holes from isolated donor sites back to the acceptor matrix to reach the anode. Collections in small molecule DDSCs are thus constrained to photogenerated holes on donors near the anode. We propose strategies to increase DDSC FF to levels comparable to bulk-heterojunction organic solar cells by decreasing the donor-acceptor highest occupied molecular orbital energy offset, or by engineering the active layer morphology so that a higher density of donors are in proximity/contact with the anode.

1. Introduction

Organic solar cells (OSCs) have been the subject of intensive investigations over the last decades because of their solution processability, energy level tunability, and materials sustainability. An OSC is fabricated by combining two organic materials: one acting as an electron donor and the other acting as the electron acceptor. In OSCs, light generates an exciton in the material and the exciton is dissociated at the donor-acceptor interface into an electron, traveling along acceptors to the cathode contact, and a hole, moving along donors to the anode contact. Most OSCs have active layers with a bulk heterojunction (BHJ) morphology [1], consisting of about half donor and half acceptor materials. In BHJ OSCs, donor and acceptor materials form interpenetrating percolative pathways, representing a compromise between fast charge collection and efficient exciton dissociation [2].

Surprisingly, OSCs fabricated using low donor concentrations (a few wt%) also exhibit decent photoresponse [3]. These small donor concentration OSCs are the subject of our present study, and we will refer to them as dilute-donor solar cells (DDSCs). The physics governing DDSC photocurrent has been under debate because it is unclear what percolative paths reach the anode for hole transport. Mechanisms like donor-donor tunneling [4] and hole back-transfer [5] have been proposed. It was recently argued hole back-transfer is more plausible than tunneling at extremely low donor concentrations (~ 1 wt%) [6]. Here we focus on the extremely dilute donor concentration (1 – 5 %) because donor domains have been reported to form percolative pathways occur around 10 wt% donors [7,8]. Three-dimensional (3D) kinetic Monte Carlo (kMC) simulations on small molecule and polymer DDSCs have also shown that holes trapped on localized donor domains can transfer to the acceptor domain and travel to the anode producing photocurrent [9,10]. One potential DDSC advantage is to produce open-circuit voltages (V_{oc}) exceeding their BHJ counterpart with comparable short

* Corresponding authors.
E-mail addresses: jwhsu@utdallas.edu (J.W.P. Hsu), william.vandenberghe@utdallas.edu (W.G. Vandenberghe).

https://doi.org/10.1016/j.nanoen.2022.107793
Received 17 April 2022; Received in revised form 6 September 2022; Accepted 7 September 2022
Available online 9 September 2022

circuit current density (J_{sc}) [3,5,11,12]. While DDSC understanding is emerging, the high V_{oc} and J_{sc} have unfortunately been accompanied by low fill factors (FFs), lower than in BHJ solar cells [3,11,13–15]. If DDSC FF can be improved, DDSC will be a very attractive solar cell technology.

While little is discussed about FF in DDSCs in literature, one trend is that FF values of DDSCs with small molecule donors are lower (~0.3) compared to those for polymer donors (~0.5) [5,6,13,16–19]. In BHJ solar cells, empirically high FFs were observed in devices with high charge mobilities [20,21], fast charge extraction [22], reduced bimolecular recombination [23–25], and long charge-separated state lifetimes [26]. However, it is not known if DDSCs' FF is determined by the same parameters.

In this paper, we investigate factors affecting DDSCs' FF. Motivated by experimental observations between solution-processed small molecule and polymer DDSCs, we calculate the current density-voltage (J-V) characteristics using kMC simulations and analyze how holes are collected at the anode. We find in small molecule DDSCs, a large electric field is required to transfer a hole from the donor back to the acceptor before recombination. The photoactive region where the large electric field can be sustained is very small and gets even smaller with increasing bias, giving rise to a low FF in small molecule DDSCs. In polymer DDSCs, a large electric field is not required as holes can avoid recombination by moving along polymer chains towards the anode. Finally, we propose that reducing the donor-acceptor highest occupied molecular orbital (HOMO) offset or increasing the density of donors near the anode can improve the FF in small molecule DDSCs, potentially reaching values close to current BHJ devices.

2. Simulation methodology

2.1. kMC algorithm

To study FF in DDSCs, we compute J-V curves using the kMC technique. The algorithm behind kMC and method of computing J-V curves are explained in Ref. [9,27]. We use the kMC framework as implemented by Albes et al. [5], which has been used in numerous studies on BHJ solar cells and DDSCs [28–31].

Our kMC model explicitly accounts for three particle types: excitons, electrons, and holes. At each kMC timestep, particles can be created, annihilated, or move. For exciton generation rates, we apply the transfer matrix method [32] on a 50 nm thick pure [6,6]-Phenyl-C71-butyric acid methyl ester ($PC_{71}BM$) film with reflections from ITO/poly(3,4-ethylenedioxythiophene):poly(styrenesulfonate) (ITO/PEDOT:PSS) anode and Ca/Al cathode contacts. Fig. S1 shows the exciton generation profile. After an exciton is generated, it can move to an adjacent site by random walk [33], decay, or dissociate when adjacent to a donor-acceptor interface. To model exciton dissociation, we assume Marcus theory [34–36]. Our dissociation rate is given in Eq. (S1). Exciton dissociation will create a hole on a donor site and an electron on an acceptor site. If an electron and hole are adjacent, they can recombine. Electron/hole transport occurs by thermally activated hopping which is modeled by the Miller-Abrahams model [27,37]. The Miller-Abraham rate is shown in Eq. (S2). The active layer is terminated by an anode and a cathode that can either inject or collect charges (only from adjacent sites). We model charge injection from Ref. [38,39].

2.2. kMC input parameterization

Fig. 1a illustrates our OSC, with an active layer, an anode, and a cathode. The active layer simulation domain measures 50 × 50 × 50 nm^3, a 1 nm lattice constant, periodic x and y coordinate boundaries, and attached electrodes on two boundaries along the z-direction. Our active layer contains acceptor molecules ($PC_{71}BM$) with 1 vol% of either small molecule or polymer donors interspersed in the acceptor material, illustrated in Fig. 1b and c. Fig. 1b illustrates the small molecule donor morphology as a uniform distribution of 1 × 1 × 1 nm^3 donors. Fig. 1c

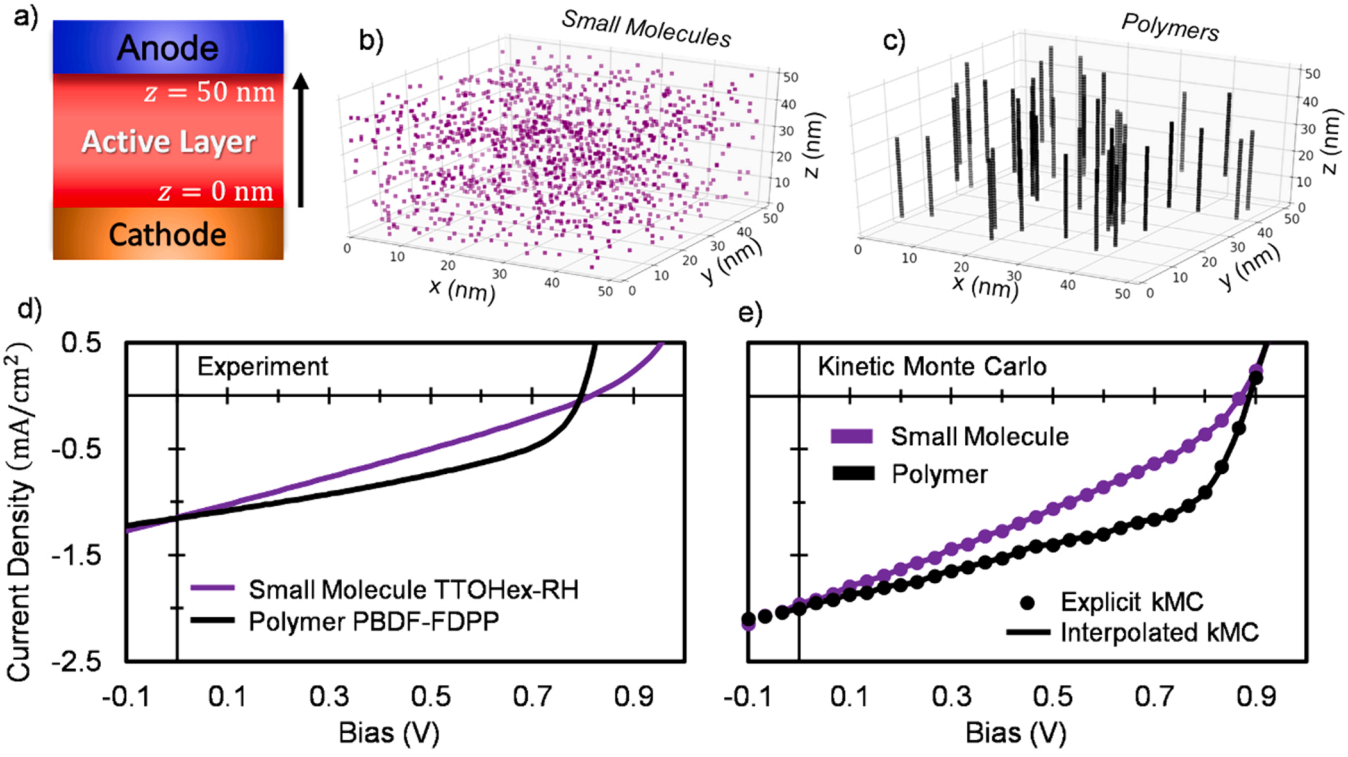

Fig. 1. (a) kMC simulated DDSC structure consisting of an active layer between an anode (z = 50 nm) and a cathode (z = 0 nm) electrode. The DDSC active layer consists of either (b) small molecule or (c) polymer donor morphologies. J-V curves from (d) experiments and (e) kMC. In kMC, the circles are results while solid lines are spline interpolations. In experiment, we use small molecule TTOHex-RH and polymer PBDF-FDPP donors to make devices with $PC_{71}BM$ acceptors. The donor concentration in the experiment and kMC simulations are respectively 1 wt% and 1 vol%.

illustrates the polymer donor morphology model as $1 \times 1 \times 30$ nm^3 linear chains perpendicular to the electrodes. We also performed simulations for, twisted polymers, illustrated in Fig. S2, but find detailed polymer morphologies do not qualitatively affect FF conclusions. To focus on the explicit differences between small molecule and polymer donors, we use the same set of physical inputs in the kMC simulation (Table S1) for both small molecule and polymer donor morphologies at a donor concentration of 1 vol%. We assume a donor-acceptor HOMO energy offset of 0.4 eV unless specified otherwise. To model hole/electron blocking layers at the cathode/anode, respectively, we parameterize an extraction rate of 5×10^6 Hz, while hole/electron extraction layers rates at the anode/cathode have an extraction rate of 1×10^{10} Hz [5].

3. Results

3.1. Experimental Results

We fabricate and measure DDSCs using four small molecule and five polymer donors in the $PC_{71}BM$ acceptor matrix. We provide detailed methodology in supporting information. The donor concentrations are 1, 2, and 5 wt%. We employ a conventional device structure with ITO/PEDOT:PSS as the anode/hole-transport-layer and Ca/Al as the electron-transport-layer/cathode. We measure J-V curves under one-sun AM 1.5 G 100 mW/cm^2 to determine J_{sc}, V_{oc}, and FF. Table 1 shows the experimental FF results of all our DDSCs while their J-V curves and J-V parameters are shown in Fig. S3 and Table S2, respectively. We find similar J_{sc} and V_{oc} ranges for small molecule and polymer DDSCs: {1.05–6.09} mA/cm^2 and {0.76–0.92} V in small molecule DDSCs and {0.54–7.63} mA/cm^2 and {0.65–0.93} V for polymer DDSCs. However, small molecule and polymer DDSCs display a notable difference in FF: a lower FF ranging between {0.26–0.35} in all small molecule DDSCs while a higher FF ranging between {0.38–0.65} in polymer DDSCs. Our FF values and the difference between small molecule and polymer donors match previous reports in literature [5,6,13,16–19].

3.2. Comparing simulation and experimental results

Fig. 1d shows experimental J-V results for 1 wt% thienothiophene-hexyloxy-rhodanine (TTOHex-RH) small molecule and poly(4,8-bis(5-(2-ethylhexyl)furan-2-yl)benzo[1,2-b:4,5-b0]difuran-alt-2,5-didodecyl-3,6-di(furan-2-yl)pyrrolo[3,4-c]pyrrole-1,4(2 H,5 H)-dione) (PBDF-FDPP) polymer DDSCs. These donors were chosen because they have similar J_{sc} and V_{oc} but different FFs, 0.27 for small molecules and 0.41 for polymers (Table 2). The FF values do not strongly depend on the donor concentration between {1−5} wt%. Fig. 1e shows the kMC J-V results for a small molecule and a polymer DDSC based on morphologies shown in Fig. 1b and c, respectively. The simulated J_{sc} and V_{oc} are the same for the small molecule and the polymer DDSCs, and the FF is 0.31 for the small molecule and 0.46 for the polymer donor. As shown, the shape of experimental J-V curves is qualitatively reproduced in the kMC simulations, with the polymer DDSC showing a higher FF. Since the kMC simulations use the same input parameters for small molecule and polymer donors, the only difference between the two DDSCs is the donor morphology.

Table 1
The experimental FF of four small molecule and five polymer DDSCs with the same $PC_{71}BM$ acceptor at donor concentrations of 1, 2, and 5 wt%. The V_{oc} and J_{sc} values of the J-V characteristics are in table S2.

Experimental Donor Morphology	Donor	FF		
		1 wt%	2 wt%	5 wt%
Small Molecule Donors	TTOHex-DC	0.28	0.27	0.26
	TTOHex-RH	0.27	0.26	0.25
	NBTT-IDD	0.28	0.27	0.35
	NBTT-Rho	0.26	0.27	0.33
Polymer Donors	PBDF-FDPP	0.41	0.51	0.63
	PThDPP-FVF	0.52	0.57	0.63
	P3HT	0.38	0.49	0.45
	PM6	0.45	0.48	0.63
	PFBT2Se2Th	0.46	0.52	0.65

Table 2
The J-V parameters extracted from the experimental and kMC simulations shown in Fig. 1d,e.

J-V Parameters	Experiment		kMC	
	Small Molecule	Polymer	Small Molecule	Polymer
FF	0.27	0.41	0.31	0.46
J_{sc} (mA/cm^2)	1.16	1.17	1.99	2.00
V_{oc} (V)	0.83	0.80	0.87	0.89

4. Why polymer donors yield a higher FF than small molecule donors

Fig. 2 shows 60–70 % of generated excitons decay before dissociating at a donor-acceptor interface in the kMC results. The remaining dissociated excitons potentially contribute to photocurrent by transferring holes onto donors and electrons on acceptors. A hole, from a dissociated exciton, has five ways to leave the DDSC (Fig. 2a) depending on if the hole originates on a donor touching an electrode or not: collection at the

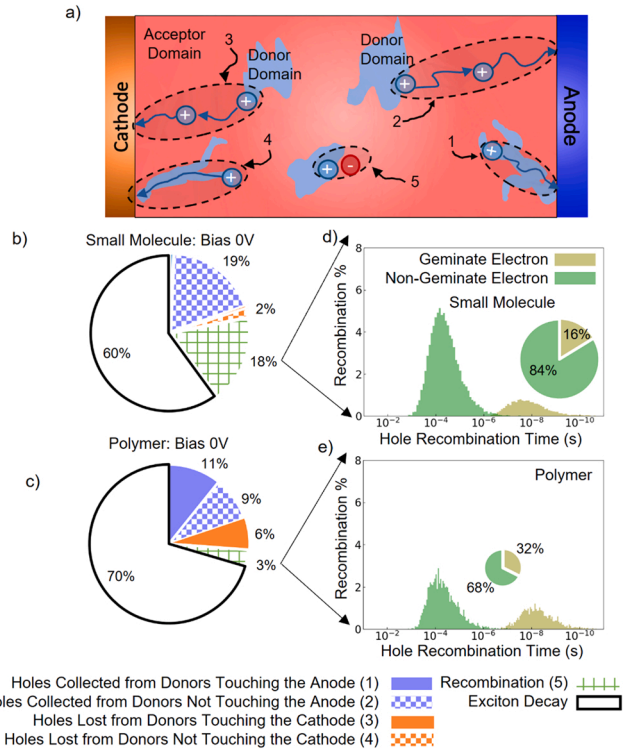

Fig. 2. Illustration of (a) five ways generated holes can leave any DDSC. A hole can originate on a donor touching the anode or not and be collected by it (process 1 and 2). A hole can also originate on a donor touching the cathode or not and be lost through it (process 3 and 4). Finally, a hole can recombine with an electron (process 5). Statistics of excitons and holes generated from dissociated excitons at 0 V bias for both (b) small molecule and c) polymer DDSCs. We normalize pie charts to the total number of excitons. Photocurrent contributions are blue while orange and green are losses. We show hole recombination distributions in d) small molecule and (e) polymer DDSCs. The smaller pie chart in (e) compared to (d) is reflective of the overall smaller amount of recombination in the former. A hole can recombine with an electron originating from the same (geminate) or a different (non-geminate) exciton.

anode (1 and 2), loss through the cathode (3 and 4), or recombination (5).

4.1. What happens to generated holes

Fig. 2b and c show the statistics of Fig. 2a along with the percentage of decayed excitons at 0 V bias. For the small molecule DDSC, most holes are collected from donors not touching the anode (19 %), which happens by back-transfer to the acceptor phase and hopping along acceptors towards the anode [5], and many recombine (18 %). For the polymer DDSC, about equal fractions of holes are collected from donors touching and not touching the anode. In the former case, holes may migrate along the polymer backbone towards the anode, while in the latter case hole back-transfer towards the anode is required. Finally, many holes are lost through the cathode (6 %), and a few recombine (3 %). In the small molecule DDSC, most holes are lost to recombination whereas in the polymer DDSC hole losses are primarily through the cathode. This exposes a stark difference in hole loss mechanisms between the small molecule and polymer DDSCs. When allowing polymers to twist (Fig. S2b), losses through the cathode remain nearly the same (6–5 %) and recombination increases moderately (3–8%) when compared to Fig. 2c.

Fig. 2d and e shows the difference between geminate and non-geminate recombination. The timescale for geminate recombination is very fast and it is very unlikely that holes exposed to geminate recombination could ever escape by traveling to a contact. Non-geminate recombination on the other hand is much slower but makes up most of the recombination events. To understand the conditions facilitating hole collection at the anode before recombination, we quantify hole transport timescales. We determine the average non-geminate recombination time $\overline{\tau}_{\mathrm{ng,rec}} = 10^{-5}$ s at 0 V bias for both small molecule and polymer DDSCs.

To quantify the competition between recombination and transport to the anode, consider that at each timestep holes can (1) hop to adjacent acceptor-sites (A), (2) hop to adjacent donor-sites (D), or (3) recombine [27]. In the small molecule DDSC case, acceptor-sites surround the donor. In this case, each hole leaves its donor by hopping to an acceptor [5]. The Miller-Abrahams hopping rate equation (Eq. S2) governing hole transitions from site i to j is

$$\frac{1}{\tau^{\mathrm{hole}}_{i\to j}} = \frac{1}{\tau^{0}_{i\to j}} exp\left(\frac{-\Delta E^{\mathrm{F+C}}_{i\to j}}{kT}\right) \tag{1}$$

where $\Delta E^{\mathrm{F+C}}_{i\to j}$ is the electric energy difference from bias, built-in and hole/electron Coulomb potentials, kT is thermal energy, and $\tau^{0}_{i\to j}$ is the hop time from sites i to j without electric fields determined from:

$$\frac{1}{\tau^{0}_{i\to j}} = a_0 \exp\left(-2\gamma_{i\to j}\Delta r_{i\to j}\right)\exp\left(\frac{-\Delta E^{\mathrm{HOMO}}_{i\to j}}{kT}\right) \tag{2}$$

where a_0 is the maximum hopping rate, $\gamma_{i\to j}$ is the inverse localization length (Eq. S3), $\Delta r_{i\to j}$ is the hopping length, and $\Delta E^{\mathrm{HOMO}}_{i\to j} = E^{\mathrm{HOMO}}_{i} - E^{\mathrm{HOMO}}_{j}$ is the HOMO offset [27]. We calculate the donor-acceptor hop time $\tau^{0}_{\mathrm{D\to A}} = 10^{-3}$ s from Eq. (2), using parameters from table S1 and $\Delta E^{\mathrm{HOMO}}_{\mathrm{D\to A}} = 0.4$ eV. In the polymer DDSC, holes can hop along the polymer chain with $\Delta E^{\mathrm{HOMO}}_{\mathrm{D\to D}} = 0$ eV, and Eq. (2) yields much shorter $\tau^{0}_{\mathrm{D\to D}} = 10^{-9}$ s.

Comparing $\tau^{0}_{\mathrm{D\to D}} = 10^{-9}$ s, $\overline{\tau}_{\mathrm{ng,rec}} = 10^{-5}$ s, and $\tau^{0}_{\mathrm{D\to A}} = 10^{-3}$ s, we find that in the absence of an electric field, recombination is faster than donor-acceptor hopping but slower than donor-donor hopping i.e., $\tau^{0}_{\mathrm{D\to D}} < \overline{\tau}_{\mathrm{ng,rec}} < \tau^{0}_{\mathrm{D\to A}}$. The much shorter $\tau^{0}_{\mathrm{D\to D}}$ compared to either of $\overline{\tau}_{\mathrm{ng,rec}}$ or $\tau^{0}_{\mathrm{D\to A}}$ suppresses recombination and is a key to understanding the larger FF in polymer compared to small molecule DDSC.

4.2. Collected holes originate near the anode in small molecules donor devices

To understand how the three time scales ($\tau^{0}_{\mathrm{D\to D}}, \overline{\tau}_{\mathrm{ng,rec}}, \tau^{0}_{\mathrm{D\to A}}$) affect photocurrent, we examine the spatial origin of collected holes. In Fig. 3a, we show the accumulated fraction of collected holes (r) at 0 V bias generated at a distance from the anode ($z = 50$ nm). Evidently a larger fraction of collected holes originate near the anode in small molecule compared to polymer DDSCs. We identify a collection-depth metric $z_{1/2}$, defined as the distance from the anode where 50 % of holes are collected ($r = 1/2$). For the small molecule DDSC, $z_{1/2} = 10$ nm (50–40 nm), and for polymer DDSC, $z_{1/2} = 18$ nm. While more excitons dissociate in the small molecule DDSC (Fig. 2b), the polymer DDSC realizes the same J_{sc} because the polymer DDSC collects holes from a larger volume in the active layer compared to the small molecule DDSC.

In Fig. 3b we show $z_{1/2}$ as a function of bias. As bias increases, $z_{1/2}$ of the small molecule DDSC sharply decreases from 10 nm to 2 nm whereas $z_{1/2}$ for the polymer DDSC remains essentially unchanged (18–14 nm). Even with bias near V_{oc}, polymer DDSC collects holes far from the anode while the small molecule DDSC only collects holes within 3 nm. These results suggest the contrasting FFs between small molecule and polymer DDSCs is governed by a difference in hole collection-depth. In particular, the relative insensitivity of $z_{1/2}$ to bias in polymer DDSC indicates hole collection remains efficient even as bias approaches V_{oc}: the signature of higher FF.

The simulation also reveals recombination is insensitive to bias for the polymer DDSC, but the small molecule DDSCs exhibit significant bias dependence, as seen in Fig. S4. This agrees with experiments showing bias dependent bimolecular recombination with low FF [24,25].

4.3. Why the small molecule donor device can only collect holes near the anode

To understand why the small molecule DDSC has a small hole-collection depth and why it is bias-dependent, we estimate the minimum electric field to free holes before recombining, or equivalently, the electric field needed for donor→acceptor hop time ($\tau^{\mathrm{hole}}_{\mathrm{D\to A}}$) to equal recombination ($\overline{\tau}_{\mathrm{ng,rec}}$) time. To this end, we equate $\tau^{\mathrm{hole}}_{\mathrm{D\to A}} = \overline{\tau}_{\mathrm{ng,rec}}$ in Eq. (1) and solve for $\Delta E^{\mathrm{F+C}}_{i\to j}$ divided by $e\Delta r_{i\to j}$:

$$\mathscr{E}_{\min} = \frac{\Delta E^{\mathrm{F+C}}_{i\to j}}{e\Delta r_{i\to j}} = \frac{-kT/|e|}{\Delta r_{i\to j}} \ln\left(\frac{\overline{\tau}_{\mathrm{ng,rec}}}{\tau^{0}_{\mathrm{D\to A}}}\right) \tag{3}$$

where e is electron charge. With Eq. (3), we calculate $\mathscr{E}_{\min} = 0.09$ V/nm. This minimum electric field can be translated to a field-limited collection length ($z_{\mathscr{E}}$) by dividing the anode to cathode work function difference ($\Delta\phi_{\mathrm{WF}} = 0.8$ V) by the minimum electric field as:

$$z_{\mathscr{E}} = \frac{\Delta\phi_{\mathrm{WF}}}{\mathscr{E}_{\min}} \tag{4}$$

For the small molecule DDSC, we find $z_{\mathscr{E}}$ as 9 nm, comparable to $z_{1/2} = 10$ nm determined in Fig. 3a.

To confirm that the small molecule DDSC has an electric field strong enough to reduce recombination, Fig. 4 presents the 0 V bias band diagram. We observe an electric field exceeding 0.09 V/nm starting at $z > 43$ nm. Thus, photogenerated holes within 7 nm from the anode travel fast enough to escape recombination whereas holes in the rest of the DDSC, are more likely to recombine before reaching the anode. It is unlikely for holes to recombine while hopping between acceptors since Eq. (2) yields $\tau^{0}_{\mathrm{A\to A}} = 10^{-10}$ s, which is much faster than recombination ($\overline{\tau}_{\mathrm{ng,rec}} = 10^{-5}$ s).

For the polymer DDSC, Eq. (3) does not apply because most collected holes avoid recombination by relying on donor→donor transport for collection (process 1 from Fig. 2a) which is insensitive to bias. For

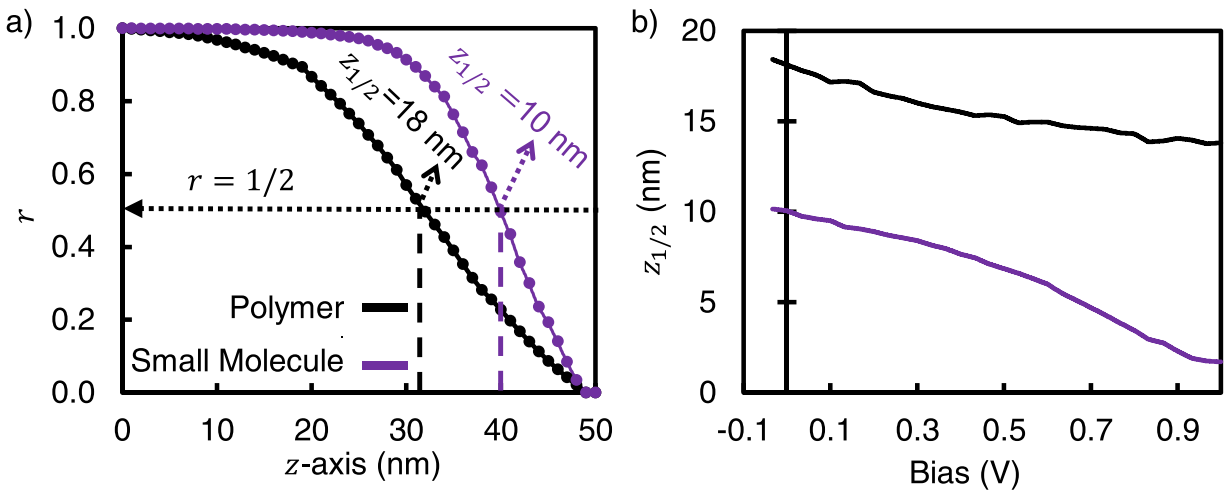

Fig. 3. (a) The cumulative hole collection ratio (r) at 0 V bias. We define r as the ratio of all collected holes originating between the anode, (z = 50 nm) and coordinate along the z-axis. We define collection-depth ($z_{1/2}$), the distance from the anode where r = 1/2. For clarity, we identify positions in a) where the collection ratio is one-half. Solid circles are individual kMC results connected by solid lines. (b) $z_{1/2}$ as a function of bias for the small molecule and polymer DDSCs.

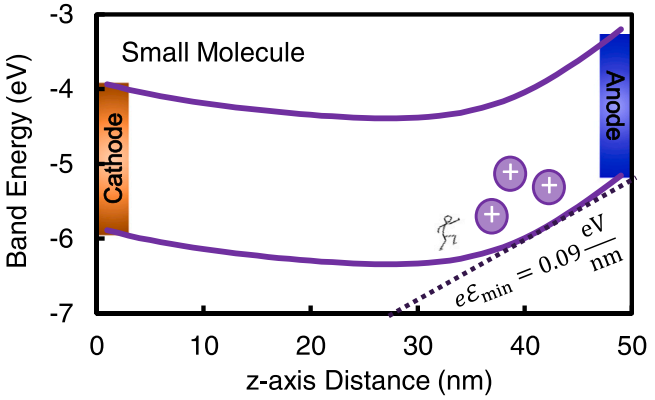

Fig. 4. The small molecule DDSC band diagram at 0 V bias. Tangent line intercepts the valence band at the location where the associated electric field can push holes from donor onto acceptors at a faster rate compared to recombination.

example, 11 % of excitons contributing to photocurrent placed holes on donors touching the anode at 0 V bias (Fig. 2c). At the built-in voltage bias of 0.8 V, the percentage is essentially unchanged at 10 % (Fig. S5). This bias insensitivity of donor→donor transport for collection is still preserved when twisting our polymers in Fig. S2b (10 % at 0 V to 9 % at 0.8 V).

As seen in Fig. 2b-c, the fraction of excitons contributing to photocurrent at 0 V bias is similar between the two device types: 19 % for small molecule and 20 % for polymer DDSCs, reflecting their comparable J_{sc}. At 0.8 V bias, the fraction of excitons contributing to photocurrent (Fig. S5) is much smaller in small molecule (3 %) compared to polymer (10 %) DDSCs, hence the much lower FF in the small molecule DDSC. This means holes can be collected even when the bias is close to the V_{oc} in polymer DDSCs. Thus, FF is regulated by the fraction of holes collected by donors touching the anode.

5. Increasing the fill factor

Based on our findings, we identify two ways to improve the FF in both small molecule and polymer DDSCs: (1) decrease the donor-acceptor HOMO offset or (2) increase the number of donors touching/near the anode. Lowering the HOMO offset decreases the donor→acceptor hop time ($\tau^0_{D\to A}$), resulting in more hole collection before recombination and thus larger collection-depths. Increasing the number of donors touching or proximate to the anode, increases the flow of holes reaching the anode without back-transferring from donors to acceptors.

5.1. Decreasing the donor-acceptor HOMO offset

In Fig. 5, we show the FF for DDSCs with donor-acceptor HOMO offset ranging from 0.4 eV to 0.2 eV. The kMC J-V curves at different HOMO offsets are in Fig. S6. A clear correlation between FF and HOMO offset is observed for both the small molecule and polymer DDSCs. For this range of HOMO offsets, the FF from small molecule DDSC increases from 0.31 to 0.59 whereas polymer DDSC FF increases from 0.46 to 0.66. Both small molecule and polymer DDSCs FF improve very significantly.

The small molecule DDSC FF improvement is entirely expected based on our previously outlined argument that photocurrent is governed by competition between recombination and hole hopping from the donor to acceptors. Decreasing the HOMO offset reduces hop time $\tau^0_{D\to A}$ and improves FF. Even in polymer DDSCs, the polymer donors not touching the anode will exhibit faster donor to acceptor hopping.

Two minor deviations are observed in the HOMO offset vs FF trend:

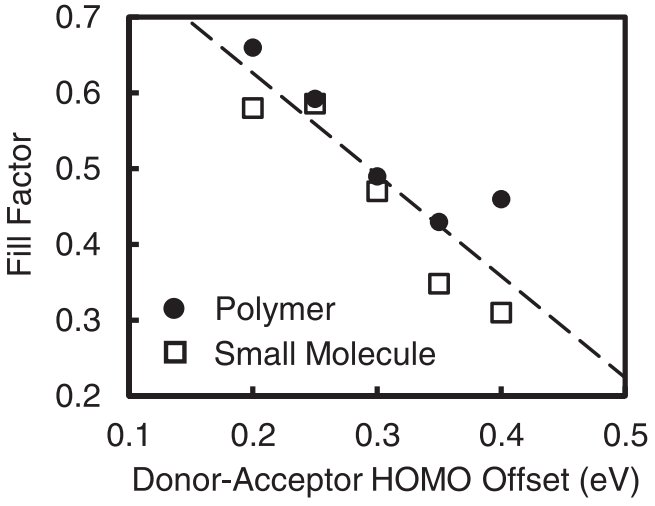

Fig. 5. FF of the small molecule and polymer DDSCs at different HOMO offsets. The dashed line is a linear fit to guide the eye.

(1) FF is lower at 0.35 eV offset in the polymer DDSC compared to 0.40 eV and (2) FF is slightly lower at 0.20 eV offset in the small molecule DDSC compared to 0.25 eV. These deviations are the result of changes in the exciton dissociation rate and losses at the cathode. In the polymer DDSC case, more dissociated excitons facilitate increased recombination at 0.35 eV offset than at an offset of 0.40 eV. Specifically, at 0.8 V bias, 9 % experience recombination (0.40 eV offset) compared to 14 % at 0.35 eV offset (Fig. S7). In the small molecule DDSC case, a larger fraction of generated holes are lost through the cathode when the offset is 0.20 eV instead of 0.25 eV. Specifically, at 0.8 V bias, 35 % (9 % / (14 % + 9 % + 3 %)) are lost through the cathode compared to 31 % when the offset is 0.25 eV (Fig. S7).

5.2. Increasing the number of donors touching the anode

In Fig. 6, we show FF from simulations with variable fraction (x) of donors touching the anode. To control x in small molecule DDSCs, we uniformly distribute donor sites in a volume between z_{min} and the anode ($z = 50$ nm), as illustrated in the insets of Fig. 6. Of the four small molecule DDSCs, three have high FF, while the last DDSC is our original from Fig. 1b and has $x = 0.02$. We also find that it is the distribution, not the aggregation, of small molecule donors that determines the FF in small molecule DDSCs (Fig. S8). For polymer DDSCs, FF increases with increasing fraction of donor chains touching the anode. Our original polymer DDSC from Fig. 1c has $x = 0.35$. The supplement describes our methodology to create all DDSC morphologies for simulation.

As seen in Fig. 6, for small molecule DDSC, FF ranges over {0.31–0.52} when x varies between {0.02–0.69} and for polymer DDSC FF ranges over {0.28–0.64} when x varies between {0.05–1.0}. For both small molecule and polymer DDSCs, FF increases with x consistent with a linear relationship (dashed line in Fig. 6). The highest FF from this linear relationship is ~0.7 ($x = 1$) which is comparable to the FFs of high performance BHJ OSCs, with past FF reports between {0.60–0.78} [22,40–42].

An experimental study of vacuum deposition of small molecule donors showed a higher FF between {0.4–0.6} [3,15,43], which agrees with our kMC small molecule DDSCs when $x > 0.2$ ($z_{min} > 40$ nm in Fig. S8). A molecular dynamics simulation study suggests that vacuum deposition facilitates donor accumulation on the anode, i.e., similar to our simulated morphology with higher x [8].

Fig. 6 shows that the fraction of donors in direct contact or proximity to the anode is a critical factor determining FF. Even when we twist polymers in Fig. S2, FF still has a linear relation with x because x controls the fraction of holes collected by donors touching the anode which we show is bias insensitive. However, the relationship between x and FF is not as strong due to increased recombination in twisted polymers.

6. Conclusion

Using kMC simulations, we explained why small molecule DDSCs exhibit a low FF and polymer DDSCs have a higher FF. From kMC hole trajectories we learned holes trapped on localized donors require a strong electric field to hop from donor→acceptor; otherwise, they will recombine and not generate photocurrent. In small molecule DDSCs, the electric field is only strong enough near the anode. We can decrease the required electric field strength by reducing the donor-acceptor HOMO offset which shorten the hole donor→acceptor hop time. Holes in polymer DDSCs do not require a strong electric field because holes originating deep in the active layer can quickly travel along polymer chains to the anode for collection.

While most currently investigated DDSCs have low FFs, our results indicate that by engineering donor materials with a more favorable donor-acceptor HOMO offset or more intimate donor contact with the anode will improve FF and may reach values of up to 0.7, being comparable to highly efficient BHJ OSCs [42]. Since kMC does not depend on the chemical nature of the acceptor, our findings should apply to

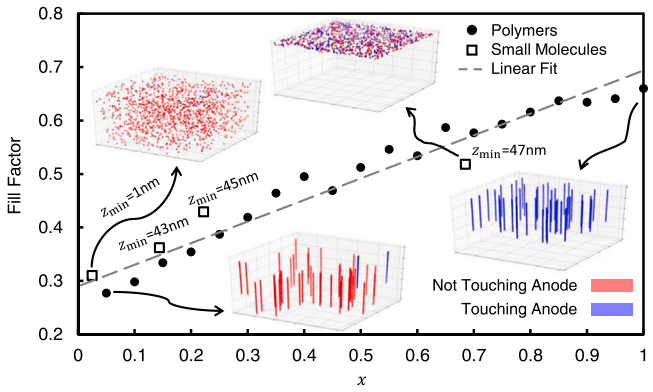

Fig. 6. The FF of 24 DDSCs: four small molecule and 20 polymer DDSCs. x is the fraction of donors touching the anode. For small molecule DDSCs, we distribute donor sites in a volume between z_{min} and the anode at 50 nm. The four insets are 3D illustrations of dilute-donor morphologies. Solid circles are polymer morphologies, and open squares are small molecule morphologies. For clarity, we labeled each small molecule data point with their respective z_{min} parameter. The dashed line is a linear fit to the polymer data points. All donor concentrations are at 1 vol%. All HOMO offsets are at 0.4 eV.

DDSCs based on non-fullerene acceptors. Thus, these results motivate further research towards developing new materials and processing techniques that can increase FF in DDSCs with high V_{oc} and J_{sc}.

CRediT authorship contribution statement

Aaron Kramer: Investigation, Methodology, Software, Writing – original draft; **Waldemar Kaiser**: Methodology, Software; **Boya Zhang**: Investigation; **Lakshmi N. S. Murthy**: Investigation; **Alessio Gagliardi**: Methodology, Software, Writing – review & editing; **Julia W. P. Hsu**: Conceptualization, Funding acquisition, Project administration, Writing – review & editing; **William G. Vandenberghe**: Conceptualization, Funding acquisition, Methodology Software, Project administration, Writing – review & editing.

Declaration of Competing Interest

The authors declare that they have no known competing financial interests or personal relationships that could have appeared to influence the work reported in this paper.

Data availability

Data will be made available on request.

Acknowledgments

We thank J.-M. Su, C.-L. Chung, and K.-T. Wong for supplying the small molecules, J. Du and M. Stefan for PBDF-FDPP and PThDPP-FVF, and F.-Y. Cao and Y.-J. Cheng for PFBT2Se2TH. This work is supported by National Science Foundation CBET-1916612. We acknowledge the Texas Advanced Computing Center (TACC) at the University of Texas at Austin for providing the high-performance computing resources that have contributed to the research results reported within this paper. URL: http://www.tacc.utexas.edu. J.W.P.H acknowledges the Texas Instruments Distinguished Chair in Nanoelectronics. A. G. acknowledges the Excellence Strategy of the Federal Government and the Länder, TUM innovation network "ARTEMIS" for funding.

Appendix A. Supporting information

Supplementary data associated with this article can be found in the online version at doi:10.1016/j.nanoen.2022.107793.

References

[1] A. Armin, W. Li, O.J. Sandberg, Z. Xiao, L. Ding, J. Nelson, D. Neher, K. Vandewal, S. Shoaee, T. Wang, H. Ade, T. Heumüller, C. Brabec, P. Meredith, A history and perspective of non-fullerene electron acceptors for organic solar cells, Adv. Energy Mater. 11 (2021) 20003570–20003612.

[2] R. Xue, J. Zhang, Y. Li, Y. Li, Organic solar cell materials toward commercialization, Small 14 (2018) 1801793–1801817.

[3] M. Zhang, H. Wang, H. Tian, Y. Geng, C.W. Tang, B. Heterojunction, Photovoltaic cells with low donor concentration, Adv. Mater. 23 (2011) 4960–4964.

[4] A. Melianas, V. Pranculis, D. Spoltore, J. Benduhn, O. Inganäs, V. Gulbinas, K. Vandewal, M. Kemerink, Charge transport in pure and mixed phases in organic, Adv. Energy Mater. 7 (2017) 1700888–1700898.

[5] T. Albes, L. Xu, J. Wang, J.W.P. Hsu, A. Gagliardi, Origin of photocurrent in fullerene-based solar cells, J. Phys. Chem. C 122 (2018) 15140–15148.

[6] L.N.S. Murthy, A. Kramer, B. Zhang, J.-M. Su, Y.-S. Chen, K.-T. Wong, W. G. Vandenberghe, J.W.P. Hsuor, Energy levels in dilute-donor organic solar cell photocurrent generation: a thienothiophene donor molecule study, Org. Electron. 92 (2021) 106137–106144.

[7] K. Ding, X. Liu, S.R. Forrest, Charge transfer and collection in dilute organic donor–acceptor heterojunction blends, Nano Lett. 18 (2018) 3180–3184.

[8] T. Lee, A. Sanzogni, N. Zhangzhou, P.L. Burn, A.E. Mark, Morphology of a bulk heterojunction photovoltaic cell with low donor concentration, ACS Appl. Mater. Interfaces 10 (2018) 32413–32419.

[9] K. Hussain, W. Kaiser, A. Gagliardi, Effect of polymer morphology on dilute donor organic solar cells, J. Phys. Chem. C 124 (2020) 3517–3528.

[10] W. Kaiser, L.N.S. Murthy, C.-L. Chung, K.-T. Wong, J.W.P. Hsu, A. Gagliardi, Origin of hole transport in small molecule dilute donor solar cells, Adv. Energy Sustain. Res. 2 (2021) 2000042–2000054.

[11] N. Yao, J. Wang, Z. Chen, Q. Bian, Y. Xia, R. Zhang, J. Zhang, L. Qin, H. Zhu, Y. Zhang, F. Zhang, Efficient charge transport enables high efficiency in dilute donor, J. Phys. Chem. Lett. 12 (2021) 5039–5044.

[12] J. Benduhn, K. Tvingstedt, F. Piersimoni, Y. S.Ullbrich, M. Fan, K.A. Tropiano, O. McGarry, M.K. Zeika, C.J. Riede, S. Douglas, S.R. Barlow, D. Marder, D. Neher, K. Spoltore, Vandewa, Intrinsic non-radiative voltage losses in fullerene-based organic solar cells, Nat. Energy 2 (2017) 17053–17059.

[13] O.J. Sandberg, S. Zeiske, N. Zarrabi, P. Meredith, A. Armin, Charge carrier transport and generation via trap-mediated optical release in organic semiconductor devices, Phys. Rev. Lett. 124 (2020) 128001–128006.

[14] M. Ghasemi, N. Balar, Z. Peng, H. Hu, Y. Qin, T. Kim, J.J. Rech, M. Bidwell, W. Mask, I. McCulloch, W. You, A. Amassian, C. Risko, B.T. O'Connor, H. Ade, A molecular interaction–diffusion framework for predicting organic solar cell stability, Nat. Mater. 20 (2021) 525–532.

[15] E. Collado-Fregoso, S.N. Pugliese, M. Wojcik, J. Benduhn, E. Bar-Or, L.P. Toro, U. Hörmann, D. Spoltore, K. Vandewal, J.M. Hodgkiss, D. Neher, Energy-gap law for photocurrent generation in fullerene-based organic solar cells: the case of low-donor-content blends, J. Am. Chem. Soc. 141 (2019) 2329–2341.

[16] L. Xu, J. Wang, M. de Anda Villa, T.B. Daunis, Y.-J. Lee, A.V. Malko, J.W.P. Hsu, Quantitative analyses of competing photocurrent generation mechanisms in fullerene-based organic photovoltaics, J. Phys. Chem. C 30 (2016) 16470–16477.

[17] D.M. Stoltzfus, C.-Q. Ma, R.C.R. Nagiri, A.J. Clulow, P. Bäuerle, P.L. Burn, I. R. Gentle, P. Meredith, Thiophene dendrimer-based low donor content solar cells, Appl. Phys. Lett. 109 (2016) 103302–103307.

[18] Bin Yang, Fawen Guo, Yongbo Yuan, Zhengguo Xiao, Yunzhang Lu, Qingfeng Dong, Jinsong Huang, Solution-processed fullerene-based organic schottky junction devices for large-open-circuit-voltage organic solar cells, Adv. Mater. 25 (2013) 572–577.

[19] Biao Xiao, Minli Zhang, Jiyan Liu, Xuebo Zhao, Hong-Bo Wang, Charge generation and recombination in high fullerene content organic bulk heterojunction solar cells, ACS Omega 2 (2017) 1702–1709.

[20] C.M. Proctor, J.A. Love, T.-Q. Nguyen, Mobility guidelines for high fill factor solution-processed small molecule solar cells, Adv. Mater. 26 (2014) 5957–5961.

[21] W. Tress, A. Petrich, M. Hummert, M. Hein, K. Leo, M. Riede, Imbalanced mobilities causing S-shaped IV curves in planar heterojunction organic solar cells, Appl. Phys. Lett. 98 (2011) 063301–063304.

[22] J. Wang, N. Yao, D. Zhang, Z. Zheng, H. Zhou, F. Zhang, Y. Zhang, Fast field-insensitive charge extraction enables high fill factors in polymer solar cells, ACS Appl. Mater. Interfaces 12 (2020) 38460–38469.

[23] A. Armin, J. Subbiah, M. Stolterfoht, S. Shoaee, Z. Xiao, S. Lu, D.J. Jones, P. Meredith, Reduced recombination in high efficiency molecular nematic liquid crystalline: fullerene solar cells, Adv. Energy Mater. 6 (2016) 1600939–1600949.

[24] Xuning Zhang, Dongyang Zhang, Qian Zhou, Rong Wang, Jiyu Zhou, Jianqiu Wang, Huiqiong Zhou, Yuan Zhang, Fluorination with an enlarged dielectric constant prompts charge separation and reduces bimolecular recombination in non-fullerene organic solar cells with a high fill factor and efficiency > 13%, Nano Energy 56 (2019) 494–501.

[25] C.M. Proctor, M. Kuik, T.-Q. Nguyen, Charge carrier recombination in organic solar cells, Prog. Polym. Sci. 38 (2013) 1941–1960.

[26] Xuning Zhang, Nannan Yao, Rui Wang, Yanxun Li, Dongyang Zhang, Guangbao Wu, Jiyu Zhou, Xing Li, Hong Zhang, Jianqi Zhang, Zhixiang Wei, Chunfeng Zhang, Huiqiong Zhou, Fengling Zhang, Yuan Zhang, On the understanding of energy loss and device fill factor trade-offs in non-fullerene organic solar cells with varied energy levels, Nano Energy 75 (2020) 105032–105041.

[27] Mosè Casalegno, Guido Raos, Riccardo Po, Methodological assessment of kinetic Monte Carlo simulations of organic photovoltaic devices: the treatment of electrostatic interactions, J. Chem. Phys. 132 (2010) 094705–094719.

[28] T. Albes, A. Gagliardi, Charge pair separation dynamics in organic bulk-heterojunction solar cells, Adv. Theory Simul. 1 (2018), 1800032.

[29] T. Albes, A. Gagliardi, Influence of permittivity and energetic disorder on the spatial charge carrier distribution and recombination in organic bulk-heterojunctions, Phys. Chem. Chem. Phys. 19 (2017) 20974–20983.

[30] Tim Albes, Paolo Lugli, Alessio Gagliardi, Investigation of the blend morphology in bulk-heterojunction organic solar cells, IEEE Trans. Nanotechnol. 15 (2016) 281–288.

[31] W. Kaiser, A. Gagliardi, Kinetic Monte Carlo study of the role of the energetic disorder on the open-circuit voltage in polymer/fullerene solar cells, J. Phys. Chem. Lett. 10 (2019) 6097–6104.

[32] G.F. Burkhard, E.T. Hoke, M.D. McGehee, Accounting for interference, scattering, and electrode absorption to make accurate internal quantum efficiency measurements in organic and other thin solar cells, Adv. Mater. 22 (2010) 3293–3297.

[33] K. Feron, X. Zhou, W.J. Belcher, P.C. Dastoor, Exciton transport in organic semiconductors: Förster resonance energy transfer compared with a simple random walk, J. Appl. Phys. 111 (2012) 044510–044516.

[34] R.A. Marcus, On the theory of oxidation-reduction reactions involving electron transfer. I, J. Chem. Phys. 24 (1956) 966–978.

[35] R.A. Marcus, Electron transfer reactions in chemistry. Theory and experiment, Rev. Mod. Phys. 65 (1993) 599–610.

[36] Thomas Unger, Stefan Wedler, Frank-Julian Kahle, Ullrich Scherf, Heinz Bässler, Anna Köhler, The impact of driving force and temperature on the electron transfer in donor–acceptor blend systems, J. Phys. Chem. C 2017 (2017) 22739–22752.

[37] A.M. Abrahams, Elihu, Impurity conduction at low concentrations, Phys. Rev. 120 (1960) 745–755.

[38] U. Wolf, V.I. Arkhipov, H. Bässler, Current injection from a metal to a disordered hopping system. I. Monte Carlo simulation, Phys. Rev. B 59 (1999) 7507–7513.

[39] V.I. Arkhipov, U. Wolf, H. Bässler, Current injection from a metal to a disordered hopping system. II, Comp. Anal. Theory Simul. Phys. Rev. B (1999) 7514–7520.

[40] Y. Wang, Y. Wang, L. Zhu, H. Liu, J. Fang, X. Guo, F. Liu, Z. Tang, M. Zhang, Y. Li, A novel wide-bandgap small molecule donor for high efficiency all-small-molecule organic solar cells with small non-radiative energy losses, Energy Environ. Sci. 13 (2020) 1309–1317.

[41] J. Yuan, Y. Zhang, L. Zhou, G. Zhang, H.-L. Yip, T.-K. Lau, X. Lu, C. Zhu, H. Peng, P. A. Johnson, M. Leclerc, Y. Cao, J. Ulanski, Y. Li, Y. Zou, Single-junction organic solar cell with over 15% efficiency using fused-ring acceptor with electron-deficient core, Joule 3 (2019) 1140–1151.

[42] G. Zhang, X.-K. Chen, J. Xiao, P.C.Y. Chow, M. Ren, G. Kupgan, X. Jiao, C.C. S. Chan, X. Du, R. Xia, Z. Chen, J. Yuan, Y. Zhang, S. Zhang, Y. Liu, Y. Zou, H. Yan, Y. Cao, Delocalization of exciton and electron wavefunction in non-fullerene acceptor molecules enables efficient organic solar cells, Nat. Commun. 11 (2020) 3943–3953.

[43] Ji-Won Seo, Jong Hun Kim, Mincheol Kim, Seon-Mi Jin, Sang-Hoon Lee, Changsoon Cho, Eunji Lee, Seunghyup Yoo, Jeong Young Park, Jung-Yong Lee, Columnar-structured low-concentration donor molecules in bulk heterojunction organic solar cells, ACS Omega 3 (2018) 929–936.

Aaron Kramer received his BS degree from the department of physics at Tarleton State University in 2016 and obtained his MS degree from the department of physics at the University of Texas at Dallas in 2018. Recently, he received a Ph.D. from the department of physics at the University of Texas at Dallas in 2022. His research interests involve modeling device physics from first principles and using Monte Carlo methods.

Waldemar Kaiser received his M.Sc. in Electrical Engineering and Information Technology in 2017 and his Dr. rer. nat. in 2021 (Thesis: Kinetic Monte Carlo Study of Charge and Exciton Transport in Organic Solar Cells) from the Technical University of Munich, Germany. He is currently post-doctoral researcher at the Computational Laboratory of Hybrid/Organic Photovoltaics (CLHYO) of the Consiglio Nazionale delle Ricerche in Perugia, Italy. His research focuses on first-principles modeling of perovskites to tailor their stability and optoelectronic properties for photovoltaic and photocatalytic applications.

Boya Zhang received her BS degree in Materials Science and Engineering from University of Shanghai for Science and Technology in 2015. She then earned her MS degree in Materials Science and Engineering from University of Rochester in 2017. She obtained her Ph.D. degree in Materials Science and Engineering from the University of Texas at Dallas in 2022. Her main research focuses on fabricating and characterizing organic solar cells for outdoor and indoor applications, as well as investigating thermal instability of perovskites in contact with metal oxides.

Lakshmi N. S. Murthy received his bachelor's degree in Metallurgical and Materials Engineering from National Institute of Technology, Trichy, India in 2015. He completed his Master's degree in 2017, and graduated with Ph.D. degree in 2021 from the Prof. Hsu's group at the University of Texas at Dallas. His research focuses on defect characterization, understanding the charge transport mechanism, and voltage losses in fullerene-based organic solar cells. He is currently working as Process Engineer at Intel Corporation.

Prof. Gagliardi research is about the development and application of numerical models for the simulation of nanostructured devices. His focus is on new solar cells (organic semiconductors based on perovskite), electrochemical systems (fuel cells, batteries) and organic semiconductor materials. The development of new models ranges from the nanoscale (Density Functional Theory, Quantum Green Functions) through the mesoscale (Kinetic Monte Carlo) to the macroscopic scale (drift diffusion, continuum models). His more recent research is on multiscale modeling for organic semiconductors and the use of machine/deep learning approaches in material science.

Julia W. P. Hsu is a Professor of Materials Science and Engineering at the University of Texas at Dallas and holds the Texas Instruments Distinguished Chair in Nanoelectronics. She received bachelor degree from Princeton University and Ph.D. degree from Stanford University, and previously worked at the University of Virginia, Bell Labs, and Sandia National Laboratories. Prof. Hsu is a Fellow of American Physical Society, American Association for the Advancement of Science, and Materials Research Society, and an International Chair Professor at Taipei Tech. She has published over 240 journal papers, 5 patents, and has given over 190 invited talks.

William G. Vandenberghe is an associate professor in the Materials Science and Engineering department at the University of Texas at Dallas. He received the M.Sc. degree in Electrical Engineering and his Ph.D. degree in Engineering from KU Leuven. His Ph.D. research was conducted at imec, an international research institute that performs research in the field of nanoelectronics. He published more than 100 research publications and received the KU Leuven research council award, and a Defense Threat Reduction Agency (DTRA) Young Investigator Award. His research focus lies in the study of electronic transport at the nanoscale.